Plasmonic Refractive Index Sensor with High Figure of Merit Based on Concentric-Rings Resonator

Zhaojian Zhang [1], Junbo Yang [2,] *, Xin He [2], Jingjing Zhang [2], Jie Huang [2], Dingbo Chen [2] and Yunxin Han [2]

[1]   College of Liberal Arts and Sciences, National University of Defense Technology, Changsha 410073, China;
      376824388@qq.com

[2]   Center of Material Science, National University of Defense Technology, Changsha 410073, China;
      yangjunbo008@sohu.com

*   Correspondence: yangjunbo008@sohu.com; Tel.: +86-158-7406-2481

Abstract: A plasmonic refractive index (RI) sensor based on metal-insulator-metal (MIM) waveguide coupled with concentric double rings resonator (CDRR) is proposed and investigated numerically. Utilizing the novel supermodes of the CDRR, the FWHM of the resonant wavelength can be modulated, and a sensitivity of 1060 nm/RIU with high figure of merit (FOM) 203.8 is realized in the near-infrared region. The unordinary modes as well as the influence of structure parameters on the sensing performance are also discussed. Such plasmonic sensor with simple framework and high optical resolution could be applied to on-chip sensing systems and integrated optical circuits.

Keywords: plasmonic sensor; high figure of merit; concentric double rings resonator

1. Introduction

Surface plasmon polaritons (SPPs) are electromagnetic fields propagating along the interface of metal-insulator, and have been widely discussed for several decades due to the ability to modulate light in nanoscale as well as break the diffraction limit [1]. Recently, many kinds of plasmonic devices have been investigated such as filters [2], absorbers [3], splitters [4] and sensors [5]. Among these, plasmonic sensors have drawn more attention, because compared with traditional optical sensors such as fiber sensors and silicon-based sensors, plasmonic sensors have much smaller size with comparable sensing performance, which means they are more suitable for integrating [6]. Various of plasmonic sensors have come out lately such as refractive index sensors [7], temperature sensors [8], phase sensors [9] and gas sensors [10].

The metal-insulator-metal (MIM) waveguide is one of the basic plasmonic waveguides with the capability to confine light within considerable propagating length [11], and many works of sensor are based on this structure [12-20]. As a sensor, it requires both high sensitivity (S) and high figure of merit (FOM) to promise an excellent performance with high optical resolution. Great efforts have been made to improve sensitivity on MIM plasmonic sensors, but longer wavelength always suffers from wider FWHM [12-15], which means lower FOM. Recently, Fano resonance has been universally applied to enhance FOM which results from structure symmetry break or dark-bright resonance interference, and it has an asymmetric spectral line shape with narrower FWHM [16-20]. But such resonance is unstable and can be easily broken due to phase or mode mismatch which could be caused by localized corrosion of structure, change of localized refractive index and so on.

In this study, a traditional MIM plasmonic sensor coupled with simple concentric double rings resonator (CDRR) is proposed. Utilizing the special supermodes, the FOM of that can be significantly improved to as high as 272.3 in the visible-light region without Fano resonance, as well as 203.8 in the near-infrared region. Such value of FOM is quite larger than other recent works [5, 7, 12-18]. The peculiar properties of CDRR supermodes and the impact of structure parameters on sensing performance are also discussed. The Finite-Difference Time-Domain (FDTD) solution is used to simulate this structure with perfectly matched layer (PML) boundary condition.

2. Structural Model and theory analysis

As shown in Fig. 1, a MIM waveguide coupled with a CDRR is proposed. The silicon substrate is plated with silver, and the waveguides are etched on the silver surface. As shown in 2D picture, the grey and white areas represent silver and air, respectively. The permittivity of air is set as $\varepsilon_i = 1$, as for silver (Ag) the Drude model is utilized as follows [2]:

$$\varepsilon_m = \varepsilon_\infty - \frac{\omega_p^2}{\omega(\omega + i\gamma)} \tag{1}$$

Here ε_∞ gives the medium constant for the infinite frequency, ω_p refers to bulk frequency for plasma, γ means damping frequency for electron oscillation, and ω shows incident light angular frequency. The parameters for silver are $\varepsilon_\infty = 1$, $\omega_p = 1.37 \times 10^{16}$ Hz, and $\gamma = 3.21 \times 10^{13}$ Hz.
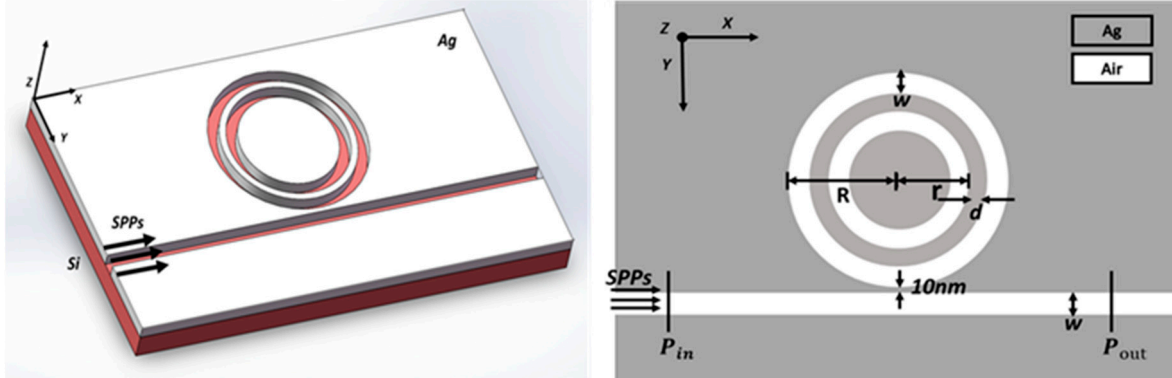
Figue.1 The 3D and 2D picture of the plasmonic sensor.

In this structure, $R = 350$nm and $r = 270$nm is the radius of the outer and inner ring, respectively. The width of the waveguide is set as $w = 50$nm, and the gap between inner and outer ring is $d = 30$nm. The gap between CDRR and bus waveguide is $g = 10$nm. To collect the incident and transmitted power, two monitors are put respectively at P_{in} and P_{out}. The transmittance of power can be calculated by $T = P_{out}/P_{in}$.

TM mode SPPs can propagate at the surface of interface in the waveguide when coupled into the MIM structure. Compared with incident wavelength the width of the bus waveguide is much smaller, so fundamental TM mode can exist only. The dispersion relation of this fundamental mode is described as follows [11]:

$$\frac{\varepsilon_i p}{\varepsilon_m k} = \frac{1 - e^{kw}}{1 + e^{kw}} \tag{2}$$

$$k = k_0 \sqrt{(\frac{\beta_{spp}}{k_0})^2 - \varepsilon_i}, \ p = k_0 \sqrt{(\frac{\beta_{spp}}{k_0})^2 - \varepsilon_m} \tag{3}$$

$$\beta_{spp} = n_{eff} k_0 = n_{eff} \frac{2\pi}{\lambda} \tag{4}$$

Here w refer to the width of bus waveguide, λ shows incident light wavelength in vacuum, ε_i and ε_m give the relative dielectric and metal permittivity, β_{spp} and n_{eff} are propagation constant and effective refractive index of SPPs, and $k_0 = 2\pi/\lambda$ means wave number.

74
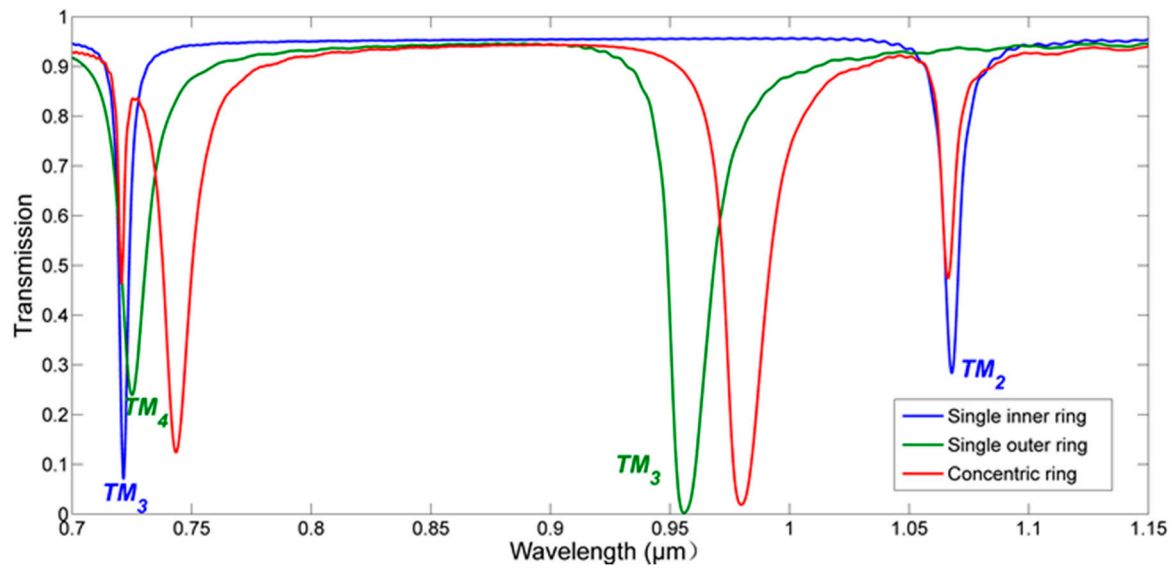
75   **Figure. 2** The transmission spectra of MIM waveguide coupled with single inner (outer) ring or
76   CDRR.

77   The transmission spectra of MIM waveguide coupled with single inner (outer) ring or CDRR are
78   shown in Fig. 2. In order to illuminate the principle of CDRR better, the gap between bus waveguide
79   and single inner (outer) ring is set as 30nm (10nm). Fig. 2 indicates that the transmission spectrum of
80   CDRR is almost the superposition of the other two spectra with slight shifts, and the FWHM of the
81   mode near 1060nm becomes narrower. For a single ring resonator, the resonance condition can be
82   described as [5]:

83
$$N\lambda = \mathrm{Re}(n_{eff})L_{eff}, N = 1, 2, 3...$$
(5)

84   Where n_{eff} refers to the effective refractive index of the ring resonator which can be solved by
85   Eq. (2–4), L_{eff} means effective perimeter, generally refers to the average of the inner and outer
86   perimeters. N refers to mode number which is an integer.
87   For the CDRR, the resonance condition is the superposition of that for single ring, and the shift
88   of resonant wavelength comes from the change of effective index of each ring resulting from the
89   interaction between each other.

90
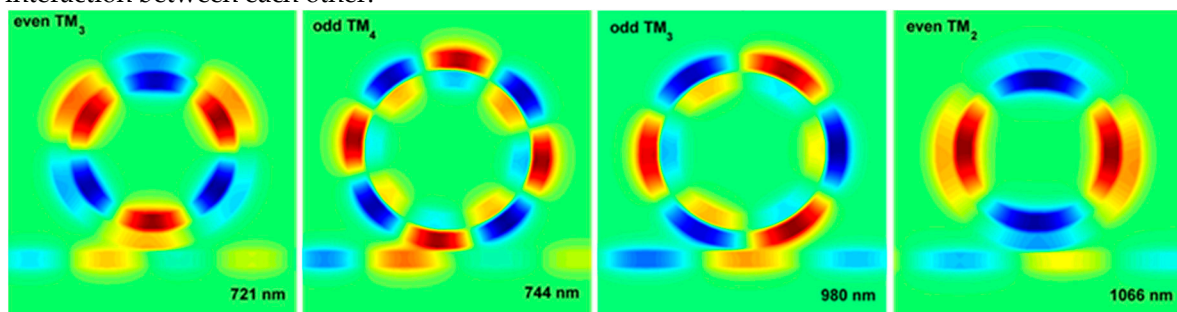
91   **Figure. 3** The supermodes of CDRR.

92   It is found that the modes of CDRR exist in the form of supermodes, which means the inner and
93   outer ring have resonance simultaneously. And the novel supermodes of CDRR are introduced as
94   shown in Fig. 3. However, we notice that there are only two kinds of supermodes: when the energy
95   is mainly trapped in outer ring, the mode in the inner ring will have anti phase; when mainly trapped
96   in inner ring, it is in phase. Refer to the supermodes between two parallel waveguides [21], the two
97   supermodes could be called odd mode (with anti-phase) and even mode (with in-phase). The
98   mechanism of such supermodes can be explained by the coupled-mode theory (CMT) [22]. The
99   propagation constant in the ring resonator can be derived with Eq. (5):

100
$$\mathrm{Re}(\beta)=\frac{2\pi\,\mathrm{Re}(n_{eff})}{\lambda}=\frac{2\pi}{\lambda}\cdot\frac{N\lambda}{2\pi R_{eff}}=\frac{N}{R_{eff}}$$
(6)

101   Where R_{eff} is the effective radius of the ring resonator, and the propagation constant of odd
102   (even) mode in the system of two parallel single-mode waveguides is as follows [22]:

103
$$\beta_{odd}=\overline{\beta}-\Delta\beta$$
(7)

104
$$\beta_{even}=\overline{\beta}+\Delta\beta$$
(8)

105
$$\overline{\beta}=\frac{\beta_1+\beta_2}{2},\quad \Delta\beta=\frac{1}{2}\sqrt{4K^2+(\beta_a-\beta_b)^2}$$
(9)

106   Here, $\bar{\beta}$ represents the average propagation constant, β_1 (β_2) is the propagation constant for a
107   single waveguide without coupling, and K is the coupling coefficient. In the condition of the
108   codirectional coupling, K is a pure imaginary number [22]. Eq. (7-8) shows that the $\mathrm{Re}(\beta_{even})$ is
109   always larger than $\mathrm{Re}(\beta_{odd})$. Since the CDRR could be considered as two parallel bend waveguides
110   with periodicity, this mode expression can also be applied. Now the CDRR system is considered as a
111   kind of single-ring resonator, the effective radius of which is determined by the energy distribution.
112   When the energy is mainly trapped in the outer side, the effective radius is larger leading to smaller
113   propagation constant according to Eq. (6), bringing about the odd mode with anti-phase in the CDRR.
114   Otherwise, it will be an even mode with in-phase.

115
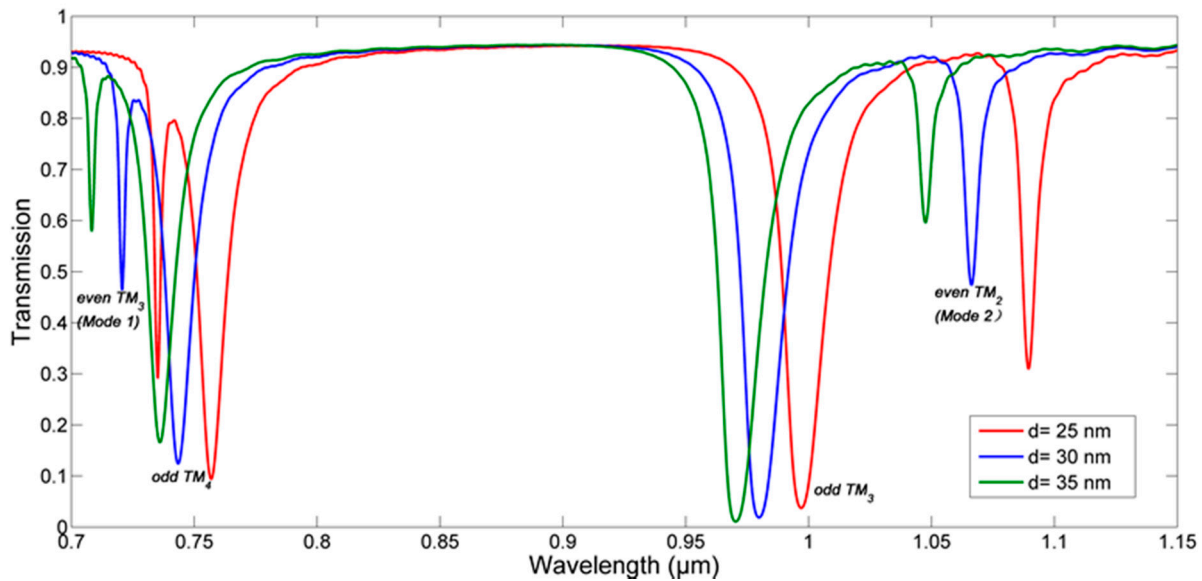
116   **Figure. 4** The transmission spectra correspond to different gaps.

117   By changing the radius of inner ring (which also means the change of the gap d), the transmission
118   spectra correspond to different gaps is obtained in Fig. 4. Obviously, the resonant wavelength will
119   have a blue shift when increasing the gap. The Fig. 5(a) shows the details, and we find that for even
120   modes, the resonant wavelength has a linear relationship with gap; for odd modes, it is nonlinear. It
121   can be explained by the effective index. When changing the radius of inner ring linearly, the effective
122   index of outer ring will be influenced and have a nonlinear change, leading a nonlinear relationship
123   between odd-mode (which can be regarded as mode of inner ring approximately according to the
124   energy distribution) resonant wavelength and gap. However, the inner ring will suffer both radius
125   and gap change, and that will keep its effective index unchanged, bringing about the linear
126   relationship between even-mode resonant wavelength and the radius of inner ring as Eq. (5). Such
127   conclusion can be useful for designing the CDRR.
128   Apparently, the even mode has much narrower FWHM, therefore the two even modes (even
129   TM_3 and TM_2) are investigated next which is assumed as mode 1 and mode 2, respectively. Fig.5 (b)
130   shows the relationship between gap d and FWHM (transmission). When increasing the gap, the

131   FWHM of even mode will be narrower, meanwhile suffering from the increase of transmission. It is
132   due to the special mode distribution of even mode, the energy of which is mainly trapped in the inner
133   ring, and the outer ring suppresses the energy loss which is beneficial for energy storage. As the inner
134   and outer rings have the same symmetry, the supermode is stable and has the single-ring mode
135   features. Such even modes are potential to generate ultra-high Q factors, which is defined as $Q = \lambda/FWHM$. With gap 30nm, the Q for mode 1 can reach 277 and for mode 2 is 205. The Q will be larger
136    $\lambda/FWHM$. With gap 30nm, the Q for mode 1 can reach 277 and for mode 2 is 205. The Q will be larger
137   with increasing gap, however there is a trade-off between Q and transmission.

138
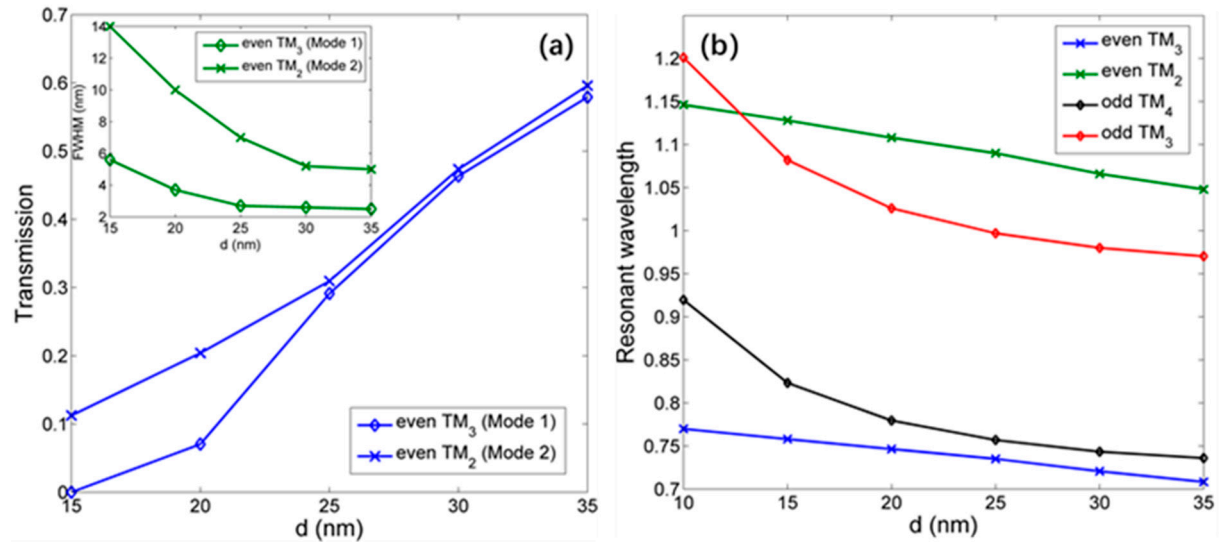
139   **Figure. 5** (a)The relationship between Transmission (FWHM) and gap. (b) The relationship between
140   resonant wavelength and gap.

141   **3. Results**

142   Considering the balance between FWHM and transmission, the gap d is chosen to be 30nm. The
143   plasmonic sensor filled with media is shown in Fig. 6, and Fig. 7 presents the transmission spectra
144   with different filling dielectric in the CDRR. The refractive index of dielectric is increased from 1 to
145   1.1 with the step 0.025, leading to a red shift of the spectra. The sensing capabilities is defined as
146   follows [23]:

147

$$S = \frac{\Delta\lambda}{\Delta n}, FOM = \frac{S}{FWHM} \tag{10}$$

148
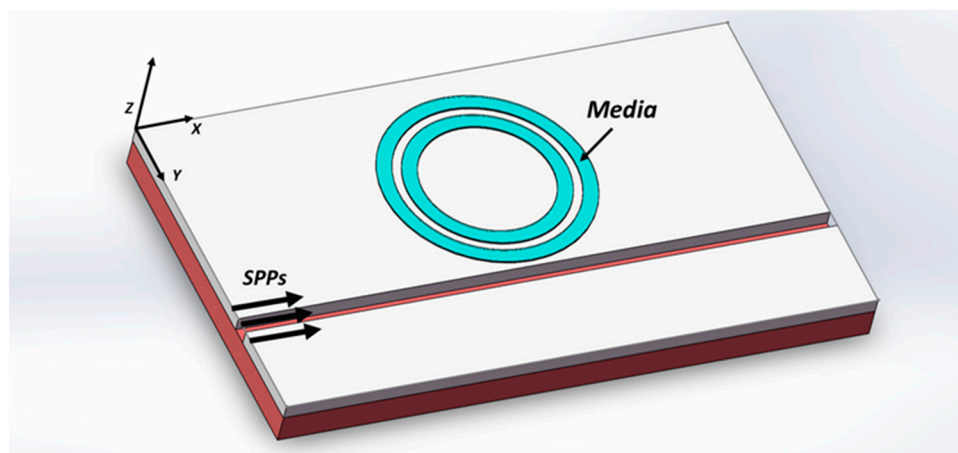
149   **Figure. 6** The 3D picture of the plasmonic sensor filled will media.

150   The sensitivity S is described as the resonant wavelength shift when the dielectric has a unit
151   change. Since the optical resolution is also crucial for sensors, a high figure of merit (FOM) is needed.

152 By fitting the line in the inset of Fig. 7, the sensitivity 708nm/RIU of mode1 and 1060nm/RIU of mode
153 2 are obtained. The FWHM of each is 2.6nm and 5.2 nm, leading to the high FOM which is 272.3 and
154 203.8, respectively. It must be mentioned that such value of FOM is quite larger than other recent
155 works as shown in Table. 1. Although some works achieved a higher figure up to hundreds of
156 thousands [19,20], the FOM definition of these works is different, which always refers to FOM^*[23].

157 **Table. 1** Comparison of S and FOM reported in various Plasmonic sensor.

Reference	S (nm/RIU)	FOM
Chen, L., et al. [5]	1496	124.6
Yan, Shu Bin, et al. [13]	868.4	43.9
Tang, Y., et al. [16]	1125	74
Zhang, Zhidong, et al. [17]	596	7.5
Zafar, Rukhsar, and M. Salim. [18]	1060	176.7
This paper	1060	203.8

158

159 Due to the higher sensitivity with excellent FOM in the near-infrared region, mode 2 is further
160 studied then. The radius of CDRR is increased with the gap d fixed at 30nm, and the spectra are given
161 in Fig. 8(a). When the outer radius raises from 350nm to 400nm with the interval 10nm, the sensitivity
162 is 1112 nm/RIU, 1152 nm/RIU, 1196 nm/RIU, 1224 nm/RIU and 1280nm/RIU respectively from Fig.
163 8(b), and FOM is 185.3, 164, 149.5, 153 and 150.4 respectively. Obviously, increasing the size of CDRR
164 can improve the sensitivity performance of the sensor with the cost of lower FOM, which may
165 respectively arise from the longer optical path and higher dissipation of energy.

166
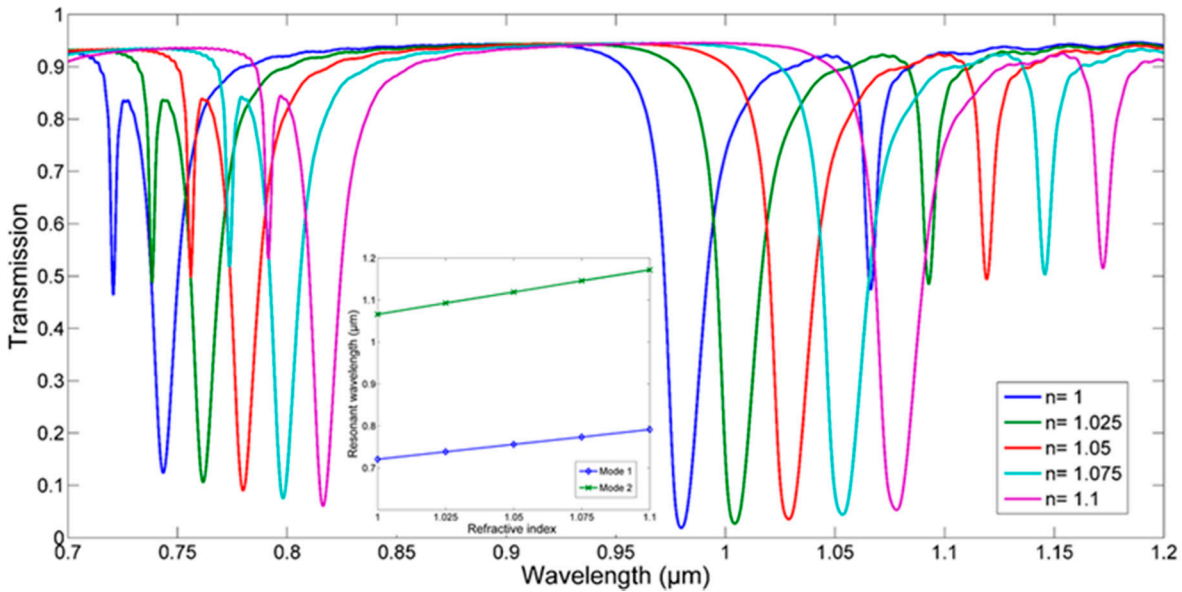
167 **Figure. 7** The transmission spectra with different filling dielectric in the CDRR. The inset shows the
168 relationship between refractive index and resonant wavelength.
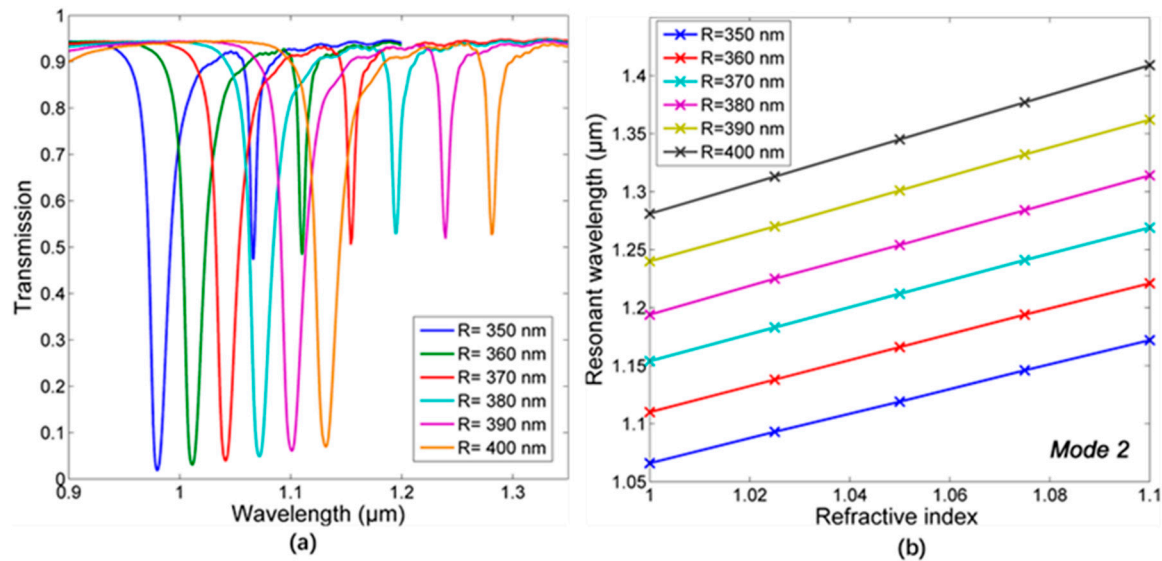
Figure. 8 (a) the spectra with different radius of CDRR. (b) the ling fitting between refractive index and resonant wavelength.

5. Conclusions

In summary, a RI sensor based on MIM waveguide coupled with a CDRR is investigated in the near-infrared region, and a high sensitivity with ultra-high FOM is obtained. The special features of supermodes in CDRR is discussed, presenting that the even mode can produce ultra-narrow FWHM. In addition, such structure also provides the concept to design a high Q microcavity. Utilizing the centrosymmetric characters of outer and inner microcavity, an ultra-high Q factor can be achieved without breaking the original mode characteristics. This device can also be used as multi band-stop filter in plasmonic system, which may have applications in integrated optical circuits.

Acknowledgments: This work is supported by the National Natural Science Foundation of China (60907003, 61671455); the Foundation of NUDT (JC13-02-13), the Hunan Provincial Natural Science Foundation of China (13JJ3001), and the Program for New Century Excellent Talents in University (NCET-12-0142).

Author Contributions: Zhaojian Zhang designed the simulations and wrote the paper; Junbo Yang disscussed and revised the paper; Dingbo Chen, Jingjing Zhang, Jie Huang, Xin He and Yunxin Han give some advises.

Conflicts of Interest: The authors declare no conflict of interest.

References

1. Ebbesen, Thomas W, A. Dereux, and C. W. Barnes. Surface plasmon subwavelength optics. *Nature* **2003**, *424.6950*, 824-830.

2. Wu, W. Ultra-high resolution filter and optical field modulator based on a surface plasmon polariton. *Optics Letters* **2016**, *41.10*, 2310.

3. Wu, D. Numerical study of an ultra-broadband near-perfect solar absorber in the visible and near-infrared region. *Optics Letters* **2017**, *42.3*, 450.

4. Yu, Y., Si J, Ning Y. Plasmonic wavelength splitter based on a metal-insulator-metal waveguide with a graded grating coupler. *Optics Letters* **2017**, *42.2*, 187.

5. Chen, L. Numerical analysis of a near-infrared plasmonic refractive index sensor with high figure of merit based on a fillet cavity. *Optics Express* **2016**, *24.9*, 9975.

6. Tong, L. Recent advances in plasmonic sensors. *Sensors* **2014**, *14.5*, 7959.

7. Y. Shen, J. H. Zhou, T. R. Liu, Y. T. Tao, R. B. Jiang, M. X. Liu, G. Xiao, J. Zhu, Z. K. Zhou, X. Wang, C. Jin, and J. Wang, Plasmonic gold mushroom arrays with refractive index sensing figures of merit approaching the theoretical limit. *Nat. Commun* **2013**, *4*, 2381.

8. Srivastava, Triranjita, R. Das, and R. Jha. Highly Sensitive Plasmonic Temperature Sensor Based on Photonic Crystal Surface Plasmon Waveguide. *Plasmonics* **2013**, *8.2*, 515-521.

203   9.   Maisonneuve, M. Phase sensitive sensor on plasmonic nanograting structures. *Optics Express* **2011**, *19.27*,
204   26318-24.

205 10.   Elsayed, Mohamed Y., Y. Ismail, and M. A. Swillam. Semiconductor plasmonic gas sensor using on-chip
206   infrared spectroscopy. *Applied Physics* **2017**, *A 123*.1, 113.

207 11.   Maier, Stefan A. Plasmonics: Fundamentals and Applications. *Springer Berlin* **2014**, *52.11*, 49-74.

208 12.   Shu, Changgan. The sensing characteristics of plasmonic waveguide with a ring resonator. *Optics Express*
209   **2014**, *22.7*, 7669-77.

210 13.   Yan, Shu Bin. A Refractive Index Sensor Based on a Metal-Insulator-Metal Waveguide-Coupled Ring
211   Resonator. *Sensors* **2015**, *15.11*, 29183-91.

212 14.   Huang, Ye Xiong. A plasmonic refractive index sensor based on a MIM waveguide with a side-coupled
213   nanodisk resonator. *IEEE, International Conference on Embedded and Real-Time Computing Systems and*
214   *Applications IEEE* **2014**, 1-5.

215 15.   Wu, Tiesheng. A nanometeric temperature sensor based on plasmonic waveguide with an ethanol-sealed
216   rectangular cavity. *Optics Communications* **2015**, *339*, 1-6.

217 16.   Tang, Y. Refractive Index Sensor Based on Fano Resonances in Metal-Insulator-Metal Waveguides Coupled
218   with Resonators. *Sensors* **2017**, *17.4*, 784.

219 17.   Zhang, Zhidong. Fano Resonance Based on Metal-Insulator-Metal Waveguide-Coupled Double
220   Rectangular Cavities for Plasmonic Nanosensors. *Sensors* **2016**, *16.5*, 642.

221 18.   Zafar, Rukhsar, and M. Salim. Enhanced Figure of Merit in Fano Resonance-Based Plasmonic Refractive
222   Index Sensor. *IEEE Sensors Journal* **2015**, *15.11*, 6313-6317.

223 19.   Zhao, X., Z. Zhang, and S. Yan. Tunable Fano Resonance in Asymmetric MIM Waveguide Structure. *Sensors*
224   **2017**, *17*, 7.

225 20.   Chen, Jianjun. Coupled-Resonator-Induced Fano Resonances for Plasmonic Sensing with Ultra-High
226   Figure of Merits. *Plasmonics* **2013**, *8.4*, 1627-1631.

227 21.   Hardy, Amos, and W. Streifer. Coupled mode theory of parallel waveguides. *Journal of Lightwave Technology*
228   **1985**, *3.5*, 1135-1146.

229 22.   Marom, E, O. G. Ramer, and S. Ruschin. Relation between normal-mode and coupled-mode analyses of
230   parallel waveguides. *Quantum Electronics IEEE Journal* **1984**, 1311-1319.

231 23.   Ameling, Ralf. Cavity-enhanced localized plasmon resonance sensing. *Applied Physics Letters* **2010**, *97.25*,
232   253116-253116-3.